Hindawi
Advances in Materials Science and Engineering
Volume 2022, Article ID 9848928, 9 pages
https://doi.org/10.1155/2022/9848928

Research Article

Mechanical Test on Aluminum Alloy with Maximal Soluble SiC Reinforcement

G. Pruthviraju,[1] Sunil G. Dambhare,[2] Bhargav Prajwal Pathri,[3] M. Ramakrishna,[1] L. Gokulanathan,[4] K. Balamurugan,[1] and W. Shumet[5]

[1]*Department of Mechanical Engineering, VFSTR (Deemed to Be University), Guntur 522213, Andhra Pradesh, India*
[2]*Dr. D. Y. Patil Institute of Engineering Management and Research, Akurdi, Pune 4110444, Maharashtra, India*
[3]*Department of Mechanical Engineering in School of Technology, Woxsen University, Hyderabad, Telangana, India*
[4]*Department of Mechanical Engineering, Sona College of Technology, Salem 636005, Tamil Nadu, India*
[5]*Department of Computer Science, Ambo University, Ambo, Post Box No. 19, Ethiopia*

Correspondence should be addressed to W. Shumet; shumet.w@ambou.edu.et

Received 5 August 2022; Revised 10 September 2022; Accepted 13 September 2022; Published 20 December 2022

Academic Editor: Temel Varol

This work deals with the characteristics of LM-13alloy under cyclic stress with and without 63% by weight of SiC-reinforced composite particle reinforcements both cast and tempered at ambient condition. The hardness of the composite sample before and after tempering was 112 HV and 134HV. The tempered sample shows 16.4% increment. UTS of base alloy and the composite was determined to be 165 MPa and 149 and 210, and 145 and 192, respectively. The UTS decreases by 12% in cast state and 8% in tempered condition. The tempered base alloy shows an increment of 21%, and the 0.25% proof stress increased by 28%. After heat treatment, the elongation at the break of the base alloy improved to 3.5%. The tempered specimen shows an increased fatigue performance of approximately 43%. The fatigue life was determined to be about 165 repetitions at the 75 MPa level of stress with 75% of UTS utilization. Decohesion of a silicon particulate interaction and in certain circumstances, the subsequent breakdown of SiC particles has led to fractures in composites. The preheated eutectic silicon that had an almost gain round shape will withstand crack growth development, as the aluminum matrix had a higher cohesive force compared to reinforced SiC particles which provide less strain increase locations. Stronger bonds among silica eutectic and aluminum matrices produced the fracture across their contact, silicon breaks owing to the application of the fatigue load and lead to specimen failure.

1. Introduction

Mechanical strength, creeping, hardness, and resistance to corrosion and wear have been improved [1]. The light matrix material's dispersion phase has been improved. The use of Al-MMCs has been increasing in recent years, as uses have been found in several automobile and spatial sectors and the overall engineering field wherever stress fracture development is just a key evaluation parameter [2]. A stress investigation of 20 vol.% of SiC particles in material composites revealed that the size of the particles played an essential effect in the regulation of the development rate of cracks [3]. There has been a comprehensive investigation of Al-SiC composite damage characteristics under high cycle load conditions [4]. Sensitivity to stress has been enhanced as SiC concentration has increased. Al-MMCs exhibited superior qualities for cracking, wear resistance, and temperature increases than homogeneous alloys [5, 6]. The isotropic characteristics of the particle-reinforced polymers are straightforward to produce using conventional foundry techniques and detect multiple to satisfy end-user needs. The nanocomposite component of metal-strengthened aluminum was shown to produce enhanced corrosion characteristics in nanoparticles due to reduced stress cycle behavior among aluminum and microparticles [7]. Sintered SiC/6061 Al combination had also been claimed to provide superior fatigue life in higher and lower fatigue failure than Al2O3/6061 composite. The author's earlier studies have been found

to improve fatigue above unreinforced-rolled composites by dispersing SiC whiskers and nanoparticles [8, 9]. In Al alloy, the Si concentration is reduced by 1.44–12.4%, as well as the product is robust to fracture development [10].

A detail-oriented stress creep process was examined that demonstrated a strong connection between the particles interface region and SiC in Al7091 and 30 vol. percent of SiC composites that led to improved ultimate load relative to Al2014-40 volume of SiC. According to moderate fatigue failure at 22°C and 190°C, Al2024-SiC particle hybrids and Al2014 alloys were noticeably affected but both elements, as well as composites outcomes, are similar [11]. For the old and aged AA6061/15% combinations of TiC peaks, the author noted a significant amount of cyclical weakening [12]. The unreinforced metal was less cyclically soft. Cyclic softness was induced by the dissolution of theta precipitates both in stressed and prestressed alloys [13]. The SiC MMCs of Al6061 volume are usually less resistant than a metal matrix to high fatigue [14]. Nevertheless, sample testing materially reacts to cyclical hardness under various aging conditions. Fracturing characteristics of whiskers reinforced MMCs. Alloy A356 strengthened with 15% SiC and 5% of fly ash particles have been shown to increase fatigue life and to enhance significantly heat therapy [15]. In comparison with unreinforced alloy, the nanocomposite IN-9052/SiCp has significantly higher fracture growth rates. The impact strength of the composite was shown to be much less than the reinforced composites [16]. The stress fracture on the base slope surface was recently reported to have been started in Mg alloy [17].In this study, the mechanical behavior of unreinforced and SiC particle-built LM13 aluminum-silicon alloy through stir casting technique has been evaluated under a range of tests under diverse circumstances. To initiate stress crash development, the impact of silicone shifting and scattered SiC particles was examined using optical scan microscopy that focused on the fracture of silicone particles, SiC fracture, and Al substrate and SiC interfacial decoherences.

2. Materials and Methods

2.1. Sample Preparation. As in the current work, highly pure silicon carbide (SiC) particulate (20–40 μm, volume of 63% wt.) and LM13 alloy were employed to make composite materials. An optic spectrometry, version: Spectra Max-X, make: Spectrograph, Germany, analyzed the chemical structure of composite materials. The elemental composition of LM13 is shown in Table 1. The Alumina crucible was used to melt base materials into an electrical arc burner. Composite of LM13-63 wt.% of SiC has been produced by stir casting. Throughout the temperature band 750–780°C, the melted LM13 alloy was heated in an alumina sink with dry nitrogen. SiC mixture was preheated to a temperature of 700°C for 12 hours and it was introduced into the melt and mechanically mixed at a rate of 700 rpm. A carbon steel mold that has a geometry of 250 mm in length and 30 mm wide was filled with the molten mix. Solidification was allowed inside the muffle furnace at 480°C for 10 hours and then dipped in an oil bath at ambient temperature. The samples are aged at a temperature of 175°C and proceeded by air chilling for 5 hours.

Table 1: Elemental composition of LM13 alloy.

Al	Si	Fe	Cu	Mg	Ni	Others
84	11	0.5	1.5	1.1	2	Remaining

2.2. Methods. An X-ray spectrometer was used for studying the crystalline structure of a pre-heated and untreated SiC. The analyzer was employed at an X-ray energy of 40 kV anode voltage with 40 mA current and 0.02° two theta per second transmission rate with CuKα radiation. The specimens were cleaned and polished to 1.0 μm for scanning electron microscope metallographic techniques. Before observing the SEM, the specimen was cleaned and etched with the Keller agent and then gold-coated. The hardness was evaluated for cast LM13 alloy, LM13 composites, and the tempered specimens using the Universal Hardness Tester at a pressure of 15 kg and a retention period of 50 seconds. The specimen was 70 mm in length, 25 mm in width, and 20 mm in thickness. The average value was given for five measurements from each specimen. Universal test machines have been used to carry out tensile observations with a crosshead speed of 1.5 mm/min. Spherical tension specimens with a 6 mm diameter and length of 30 mm were prepared and evaluated following ASTM B 557. Instron universal hydraulic inspection equipment that has a capacity of 100 kN integrated with a computer and software for data extraction was used for the fatigue test. A tensile-compressive load with a continuous frequency was applied to the load control system. The added load characteristics that include stress range, stress frequency, and fatigue stress ratio were defined by the high and low levels of stress. At 0.8 Hz frequency and a strain rate $R = 0.15$, fatigue tests were performed. The S-N curves are chosen for load disturbances between the UTS and fatigue threshold. Experiments with a specimen failure above 50,000 cycles were neglected. To avoid errors, specimens that failed in the test conditions were eliminated. The specimens that failed in the strain gauge have been considered in the current report. Specimen breakdown in the grip region has been noted in all studies not more than 2–3 times in particular for LM/63% of SiC composite alone. The failure could have been caused by SiC particle segregation. The sample dimensions were produced according to standard ASTM E466. The mechanism and location of the crack propagation were assessed by the examination of surface defects; thus, the samples were cut into tiny sizes, utilizing a slow-speed diamond cutting for microstructural analysis. SEM was used to analyze the crystalline structure and fracturing substrates of all test case samples.

3. Results

3.1. X-Ray Diffraction. SiC annealed was verified for the alteration of crystalline structure. The SiC particles were preheated for 20 minutes to wetness and triggered the

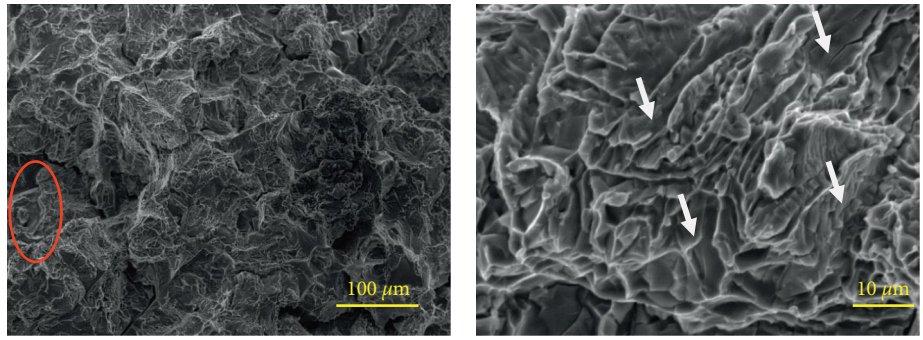

(a) (b)

Figure 1: Cast LM-13 alloy (a) aluminum dendrites surrounded by Si particles (b) Si eutectic is present in plastic form with microcrack.

energies of the surfaces well before particles are added to the molten Al melt. SiC wave was shown in the X-ray diffraction study. The XRD patterns studies show that when SiC particles have been preheated, there was no indication of phase alteration and SiC particles remained durable at 750°C.

3.2. Microscopy

3.2.1. Microstructure of Base Matrix Materials and Tempered Condition. In the case of casting, the microstructure of an LM13 is shown in the intergranular areas as illustrated in Figures 1(a) and 1(b). Figure 2(a) exhibits a better resolution image of 80–90 μm in length and 1–3 μm in height, platform-formed eutectic silicon. The thermal process of tempered LM13 resulted in the fracturing of austenite silicon into a near-sphere shape. The typical tempered heat-treated alloy microstructure is shown in Figure 2(a). In the inter-dendritic gap and between the dendrites, it displays aluminum dendrites and approximately round eutectic silicon. The relatively close spherical shape of silicon is well seen in a higher resolution image, Figure 2(b).

3.2.2. Microstructure of Composite Specimen and Tempered Condition. Figure 3(a) depicts the uniform distribution of SiC inside the base matrix. The remaining characteristics are virtually identical to those of an unreinforced matrix. There was no evidence of SiC particle separation. The interaction between the base matrix and SiC is illustrated in Figure 3(b). At the contact, plate-shaped equiaxed silicon could be observed. The distributed SiC particles inside the tempered alloy matrices are shown in Figure 3(c). The SiC samples were observed to be surrounded by a near-spherical eutectic transition. The interaction between both the tempered base matrices and the SiC particles is shown in Figure 3(d).

3.3. Mechanical Properties

3.3.1. Hardness. The Vickers Scale was used to assess the degree of hardness, with an average of five recorded values. The hardness of the base alloy was determined to be 91 HV, after tempering it was enhanced to 114 HV with an increment of 20%. The hardness of the composite sample before and after tempering was 112 HV and 134 HV. Figure4 following high temperature and dispersed 63 wt% SiC particles, the Vickers hardness of tempered samples was improved to 16.4%. Similar observations are recorded by Parapurath et al. [18].

3.3.2. Tensile Properties. The 0.25% proof stress and UTS of base alloy and its composite both in casting and tempered conditions are shown in Figures 5(a) and 5(b). In both test cases, the UTS of base alloy and the composite was determined to be 165 MPa and 149 210, and 145 and 192, respectively. The UTS decreases by 12% in cast state and 8% in tempered condition when 63 wt.% of SiC is dispersed in LM13 alloy. The tempered base alloy shows an increment of 21%, and the 0.25% proof stress increased by 28%. After heat treatment, the elongation at the break of the base alloy improved to 3.5%. The change in the microstructure due to the heat treatment improved the tensile property of the samples [19]. A similar pattern may also be for both test cases. The percentage elongation is determined to be negligible and remains the same with test conditions as 1.5%.

3.4. Fatigue Study. Stresses varying between 95 MPa and 185 MPa were used during the fatigue testing. Figure 6 depicts the S-N curve. As this was the usual sample's fatigue lifetime, the duration utilized for fatigue failure was confined to 50000 cycles. Throughout the fatigue test, 50000 repetitions of cast Al-Si alloy at a stress level of 104 MPa with the UTS utilization of 70% were accomplished. The cycles to fracture dropped to 41500 when the stress was raised to 139 MPa with a UTS utilization efficiency of 80% which can be referred from Figure 6. Similarly, based on the increment stress conditions and UTS efficiency, the cycles to failure decrease. At a stress level of 166 MPa, the specimen can able to survive for 319 cycles with the maximum UTS utilization efficiency of 94% before failure. Consequently, with a load of 142 MPa, the greatest number of cycles survived by the Al-Si alloy at a tempered state was 49000 cycles. Increased stress at 158 MPa reduced fatigue life to 35000 cycles with an increment of UTS utilization to 58%. The failure occurred at just 900 cycles at 169 MPa when the UTS utilization % was 67. Based on the comparison report for the test condition of

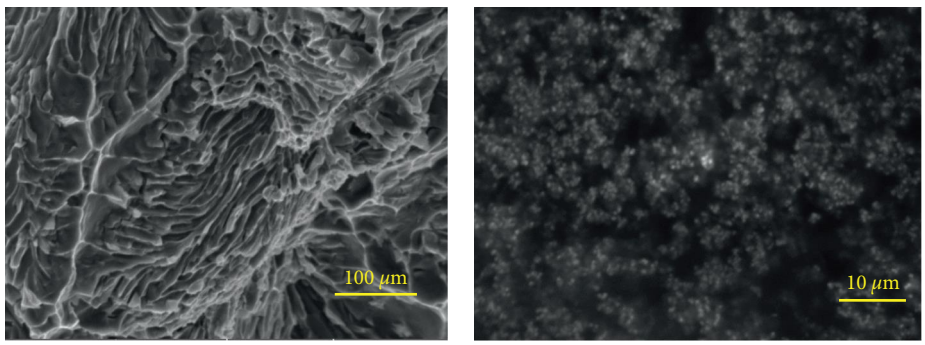

(a) (b)

Figure 2: LM13 composite microstructure at tempered conditions: (a) sphere shape Silicon between and around the aluminum dendrites (b) High resolution image showing spherical eutectic shape Silicon element.

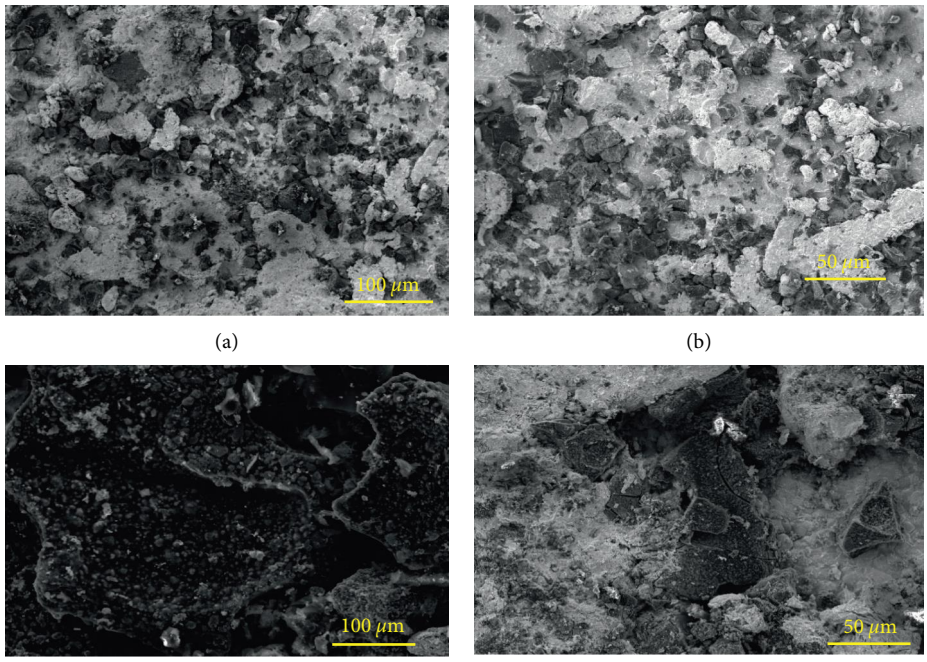

(a) (b)

(c) (d)

Figure 3: (a) Composite with distribution of SiC, (b) Contact point of base matrix specimen with SiC, (c) Tempered composite with the distribution of SiC,(d) Contact point of the tempered composite specimen with SiC.

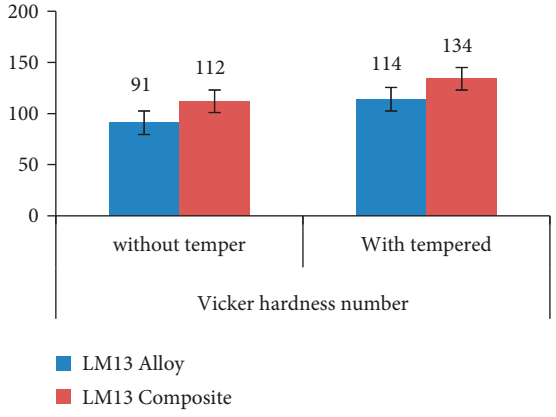

Figure 4: Hardness of the test samples.

158 stress levels the specimens can able to withstand fatigue life of 19900 and 35000, respectively before failure. As a result, the tempered specimen shows an increased fatigue performance of approximately 43%. The result obtained in this observation was more likely near to the Shanyavskiy and Soldatenkov observations [20].

The composite is sustained at 47000 cycles at a stress level of 61 MPa with 42% of utilization. Its load-bearing capacity was reduced to 12800 cycles when the stress level was increased to 73 MPa with 60% of UTS. The fatigue life was determined to be about 165 repetitions at the 75 MPa level of stress with 75% of UTS utilization. Marcelino dos Santos et al. stated that dynamic bond strength tests, using cyclic loading, should be more clinically relevant than static bond

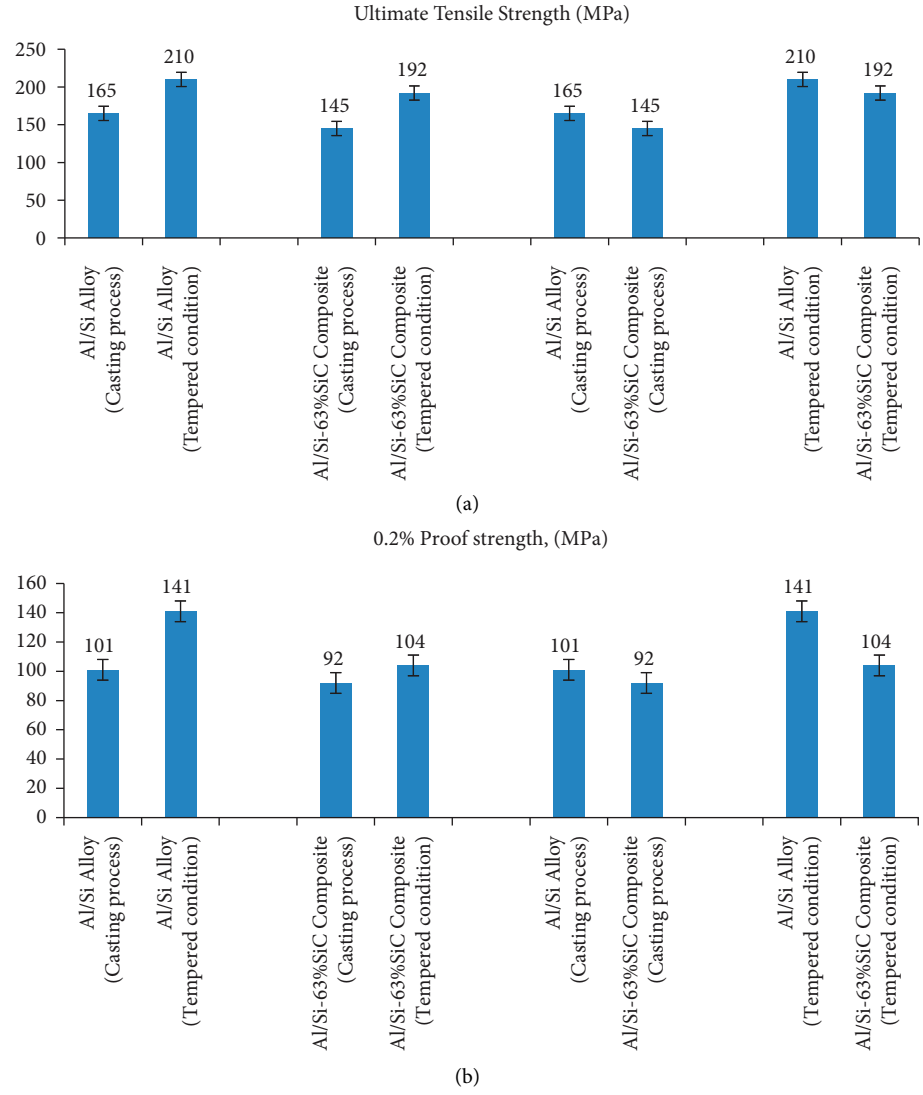

Figure 5: (a) UTS of test case specimens (b) 0.25% of proof stress observations.

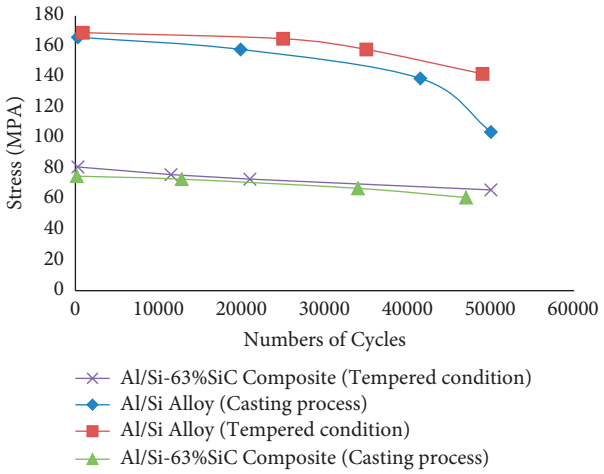

Figure 6: S-N curve of Al-Si alloy and Al-Si/63% SiC composite at various states.

strength tests [21]. Furthermore, at a stress level of 66 MPa, composites demonstrated a fatigue performance of 50000 cycles in tempered conditions at UTS utilization of 46%. The duration to breakdown was reduced to 312 cycles at 81 MPa with UTS utilization of 57%. The load capacity of the composite was reported to increase by 39% after tempering. Comparing the stress rate when temper treated and untreated composite at 73 MPa, it withstands 21000 and 12800, repetitive cyclic loads [22].

3.5. *Fatigue Failure Analysis for Tempered Condition and Untreated Specimens*

3.5.1. Al-Si Alloy. At reduced stress magnitudes, the surface morphology of the casted Al-Si alloy state displayed patterns of stress topography and subsequent cracks that can be verified in Figure 7(a). The microcracked surface displayed the intensity of stress magnitudes, but not at lower stress

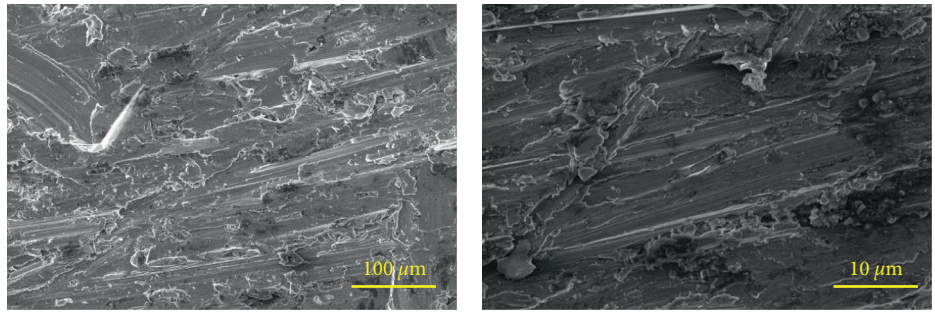

(a) (b)

Figure 7: (a) Fatigue failure surfaces for Al-Si alloy with striations and cleavage fracture (b) Fatigue failure surfaces for Al-Si/63%SiC with striation mark.

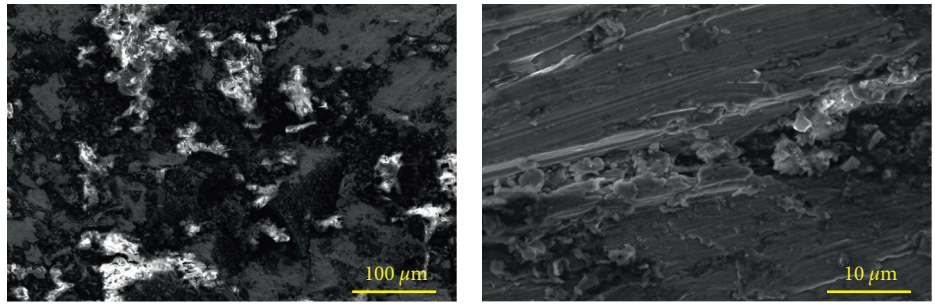

(a) (b)

Figure 8: Case Al-Si/63% SiCtest specimen (a) Initiation of Fatigue crack (b) Deformation in particle-matrix region.

amplitudes. From Figure 7(a), the shear material of the silicon particles caused by quasi-cleavage fracturing is witnessed. Figure 7(b) illustrated that the stress deformation of tempered treated Al-Si alloy was likely to be similar to cast alloy. The spherical morphology of silicon prevents the samples from failing prematurely at lower stress. This results in the development of tiny bulges that can be verified in Figure 7(b). These dimples are dispersed equally after periodic strain, resulting in a less rough microscopic texture in tempered specimens. Decohesion of nearly round silicon caused the bulge structures in the casted Al-Si alloy, whereas no breakage was detected in temper specimens.

3.5.2. Al-Si/63% SiC Composite. The surface morphology of a casting Al composite with stress streaks and silicon particles is shown in Figure 8(a). The matrix was primarily used to spread the fatigue fractures. Cracking and progression were caused by an increase in shear stress at the particulate boundary. Decohesion at the contact happened because of the developed shear stress and it can be verified from Figure 8(b). According to a new analysis, the fracture in 7075–T6 Al alloy–SiC composite is caused by the fracturing of SiC particles, the Al matrix, and the Al-SiC contact [22]. Figure 8(b) shows the particle-matrix interaction. Because of the increased stress intensity, big-size SiC particles have a greater chance of particle breakage. The amount of stress in particulates was anticipated to be greater than that in tiny SiC particles. As a result, big particulate breakage happened at low load applied conditions. The fracture microstructure of the composite surface after temper was exhibited in Figure 9(a). Fracture begins at the contact point of the matrix and the SiC particles. The bond exhibits seem to be in fine condition, with no interfacial voids which can be confirmed through Figure 9(b). Following repetitive load conditions, the fracture begins in the weaker area, namely, the particle-matrix interface. Interface decohesion occurred from the fracture growth.

4. Discussion

4.1. Relation Exists between Mechanical Property and Microstructure. Al dendrites (tree-like structure) and silicon in the inter-dendritic and also across the dendrites are visible in the microstructure of cast Al-Si alloy. The gap between adjacent neighboring dendrites arm gap was determined to be nearly 35 μm. From the earlier studies, unlike Al-Cu alloys, Al-Si alloys are aberrant eutectics wherein aluminium and silicon elements in the composition itself will nucleate separately. Also, silicon develops an anisotropic phase through the twin planes edge process into a plate or a needle shape with sharp edges [23]. A similar observation was recorded in Figure 1(b) for Al-Si cast alloy. The catastrophic failure was mainly caused because of the formation of such silicon morphology in the base alloy. Through the earlier reports and the morphological studies of Al-Si alloy, it could

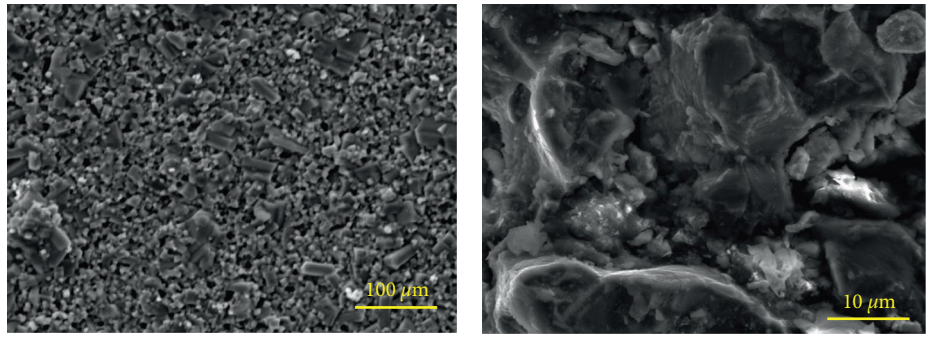

(a) (b)

Figure 9: Tempered Al-Si/63%SiCtest specimen (a) Matrix failure (b) debonding between the matrix and reinforcements.

be convenient to understand the reason for the reduction in deflection rate in Al-Si alloy which is recorded to be nearly 1.5 mm at the applied load condition.

Generally, an Al-Si bidirectional alloy is not suitable for heat treatment as it is employed in its cast state. To improve the properties of these alloy, materials such as Cu, magnesium, and nickel are blended which could enable the binary alloy thermal treatable. A comprehensive study on the thermal treatment of Al-Si alloy has not been reported elsewhere. In the proposed work, after tempering, the UTS of the cast alloy improved from 165 MPa to 210 MPa. following thermal treatment, the increase in UTS observed was attributable not only to precipitate hardening but to a modification in silicon shape from plates to nearly sphere and this can be verified from Figures 2(a) and 2(b). The introduction of Ni to the alloy resulted in the formation of $NiAl_3$ followed by thermal processing had improved the thermal stability. Following thermal processing, the cast alloy showed an improved hardness from 91 to 114 HV. Furthermore, an enhancement in the proof stress was observed from 101 to 141 GPa. For its greater surface potential, the sharp-edged plate-shaped silicon phase in the aluminum alloy was thermodynamically unstable. In comparison to a central section of the silicon plates, maximum stress is likely higher at these sharp corners [24].

As either a consequence of the liquid diffusion, sharp edges melt and deposit in the center parts of the plate's structure. The high temperature resulted in the development of nearly spherical silicon particles. It results in the silica materials size having a more homogeneous grain size as well as a lower aspect ratio. The inter-silicon particle spacing decreased when the needle-shaped silica changed into a spherical structure. Throughout the cast specimen, the average inter-silicon particle spacing was about 3 μm, but in the tempered specimens, the distance was decreased to 2.5 μm. The inter-particle spacing was decreased, and silicon was spheroidized, which decreased the number of potential stress accumulation locations. When contrasted to the cast alloy, the precipitate hardening produced by tempering treatment resulted in an excellent gain in hardness, toughness, and flexibility, including fatigue resistance. With the increment in the stress at the interfacial regions, the functionality decohesion occurred causing the composite specimens to premature failure. However, in the tempering state, the same behavior was identified. The improvement in the UTS and hardness was observed when compared with the untreated alloy.

4.2. Fatigue Property of Al-Si Alloy. When compared to cast alloy, thermal treatment enhanced the fatigue performance of the alloy and its composites. Finer-size particle-reinforced Al-Si-SiC composites have been found to have greater toughness than coarse matrix composites in certain situations [25]. The enhanced fatigue life was identified by raising the SiC particle percentage in Al-Mg alloy to 20% as the applied load is transferred from the matrix to a SiC particle [26]. The fatigue strength of the composite is understood to be strongly dependent upon applied load related to component phases. In cast Al-Si alloy, the silicon creates a plate-shaped morphology that acts as a stress raiser [27]. During the application of the tensile stress, fracture crystallographic planes near the stress riser increases and it is propagated, the final specimen failed. Sharp-edged silicon became almost spherical after tempering as the applied load effect was decreased with the change of silicon structure and increased fatigue property. The boundary here between matrix alloy and ceramics component functioned as both a possible location for decohesion throughout the instance of SiC particles distributed in Al-Si alloy which was shown in Figure 3. The junction served as a possible location for crack formation before fracture development and failure.

5. Conclusions

Al-Si alloy and Al-Si/63% of SiC composite were prepared through the stir casting technique where one set of samples was tempered for 175°C. The evaluations of the samples are performed in terms of characterization studies, hardness, tensile, and fatigue tests. Temper treatment converted the sharp-edged plate-shaped silicon into a proximity state. The shape of the silicon component was altered, which enhanced the casting alloy's durability and hardness. The hardness of the composite sample before and after tempering was 112 HV and 134 HV. The tempered samples were improved to 16.4%. The UTS decreases by 12% in cast state and 8% in

tempered condition. The tempered base alloy shows an increment of 21%, and the 0.25% proof stress increased by 28%. After heat treatment, the percentage elongation is determined to be negligible and remains the same with test conditions as 1.5%. Based on the comparison report for the test condition of 158 stress levels, the specimens can be able to withstand fatigue life of 19900 and 35000, respectively before failure. As a result, the tempered specimen shows an increased fatigue performance of approximately 43%. The composite load-bearing capacity was reduced to 12800 cycles when the stress level was increased to 73 MPa with 60% of UTS. The fatigue life was determined to be about 165 repetitions at the 75 MPa level of stress with 75% of UTS utilization.

Data Availability

There are no relevant data to be made available.

Conflicts of Interest

The authors declare that they have no conflicts of interest.

References

[1] S. D. Wang, M. Y. Wu, D. K. Xu, and E. H. Han, "Improving corrosive wear resistance of Mg-Zn-Y-Zr alloys through heat treatment," *Journal of Magnesium and Alloys*, 2021.

[2] J. V. Suman, K. K. Cheepurupalli, and H. L. Allasi, "Design of polymer-based trigate nano scale fin FET for the implementation of two-stage operational amplifier," *International Journal of Polymer Science*, vol. 2022, Article ID 3963188, 12 pages, 2022.

[3] P. Garikapati, K. Balamurugan, T. P. Latchoumi, and R. Malkapuram, "A cluster-profile comparative study on machining AlSi7/63% of SiC hybrid composite using agglomerative hierarchical clustering and K-means," *Silicon*, vol. 13, no. 4, pp. 961–972, 2021.

[4] S. Bahl, "Fiber reinforced metal matrix composites-a review," *Materials Today Proceedings*, vol. 39, pp. 317–323, 2021.

[5] T. Yeshiye and M. Gizaw, "A review on Effects of reinforcements on properties and wear behavior of aluminium metal matrix material," *International Journal of Renewable Energy Technology*, vol. 2, no. 6, 2021.

[6] S. Khelge, V. Kumar, V. Shetty, and J. Kumaraswamy, "Effect of reinforcement particles on the mechanical and wear properties of aluminium alloy composites: Review," *Materials Today Proceedings*, vol. 52, pp. 571–576, 2022.

[7] K. Balamurugan, M. Uthayakumar, M. Ramakrishna, and U. T. S. Pillai, "Air jet Erosion studies on mg/SiC composite," *Silicon*, vol. 12, no. 2, pp. 413–423, 2020.

[8] A. Thakur, R. S. Joshi, and A. Singh, "A brief review on mechanical properties of Al-MMCs fabricated by stir casting route & applications," *E3S Web of Conferences*, vol. 309, 2021.

[9] S. Gowthaman, K. Balamurugan, P. M. Kumar, S. A. Ali, K. M. Kumar, and N. V. Ram Gopal, "Electrical discharge machining studies on monel-super alloy," *Procedia Manufacturing*, vol. 20, pp. 386–391, 2018.

[10] Y. Chen and X. Zhang, "Study on the cutting mechanism of SiCp/Al considering particle size and distribution," *International Journal of Advanced Manufacturing Technology*, vol. 115, no. 4, pp. 1211–1225, 2021.

[11] M. Tayebi, M. Tayebi, M. Rajaee, V. Ghafarnia, and A. M. Rizi, "Improvement of thermal properties of Al/Cu/SiC composites by tailoring the reinforcement microstructure and comparison to thermoelastic models," *Journal of Alloys and Compounds*, vol. 853, Article ID 156794, 2021.

[12] B. A. Kumar, M. M. Krishnan, A. F. Sahayaraj et al., "Characterization of the aluminium matrix composite reinforced with silicon nitride (AA6061/Si3N4) synthesized by the stir casting route," *Advances in Materials Science and Engineering*, vol. 2022, Article ID 8761865, 8 pages, 2022.

[13] S. Sharma, J. Singh, M. K. Gupta et al., "Investigation on mechanical, tribological and microstructural properties of Al–Mg–Si–T6/SiC/muscovite-hybrid metal-matrix composites for high strength applications," *Journal of Materials Research and Technology*, vol. 12, pp. 1564–1581, 2021.

[14] K. Maleki, A. Alizadeh, and M. Hajizamani, "Compressive strength and wear properties of SiC/Al6061 composites reinforced with high contents of SiC fabricated by pressure-assisted infiltration," *Ceramics International*, vol. 47, no. 2, pp. 2406–2413, 2021.

[15] M. Dehghanzadeh Alvari, M. Ghassemi Kakroudi, B. Salahimehr, R. Alaghmandfard, M. Shahedi Asl, and M. Mohammadi, "Microstructure, mechanical properties, and oxidation behavior of hot-pressed ZrB2–SiC–B4C composites," *Ceramics International*, vol. 47, no. 7, pp. 9627–9634, 2021.

[16] T. P. Latchoumi, K. Balamurugan, K. Dinesh, and T. P. Ezhilarasi, "Particle swarm optimization approach for waterjet cavitation peening," *Measurement*, vol. 141, pp. 184–189, 2019.

[17] N. Ashrafi, A. H. M. Ariff, M. Sarraf, S. Sulaiman, and T. S. Hong, "Microstructural, thermal, electrical, and magnetic properties of optimized Fe3O4–SiC hybrid nano filler reinforced aluminium matrix composite," *Materials Chemistry and Physics*, vol. 258, Article ID 123895, 2021.

[18] S. Parapurath, L. Jacob, E. Gunister, and N. Vahdati, "Effect of microstructure on electrochemical properties of the EN S275 mild steel under chlorine-rich and chlorine-free media at different pHs," *Metals*, vol. 12, no. 8, p. 1386, 2022.

[19] S. Balaji, P. Maniarasan, S. V. Alagarsamy, A. M. Alswieleh, V. Mohanavel, and M. Ravichandran, "Byong-Hun Jeon, and Haiter Lenin Allasi, optimization and prediction of tribological behaviour of Al-FeSi alloy-based nanograin-refined composites using Taguchi with response surface methodology," *Journal of Nanomaterials*, vol. 2022, Article ID 9733264, 2022.

[20] A. A. Shanyavskiy and A. P. Soldatenkov, "Metallic materials fatigue behavior: scale levels and ranges of transition between them," *International Journal of Fatigue*, vol. 158, Article ID 106773, 2022.

[21] J. R. Marcelino dos Santos, M. F. Fernandes, V. M. D. O. Velloso, and H. J. C. Voorwald, "Fatigue analysis of threaded components with Cd and Zn-Ni anticorrosive coatings," *Metals*, vol. 11, no. 9, p. 1455, 2021.

[22] A. Kumar, S. Kumar, N. K. Mukhopadhyay, A. Yadav, V. Kumar, and J. Winczek, "Effect of variation of SiC reinforcement on wear behaviour of AZ91 alloy composites," *Materials*, vol. 14, no. 4, p. 990, 2021.

[23] K. Balamurugan, M. Uthayakumar, S. Sankar, U. S. Hareesh, and K. G. K. Warrier, "Predicting correlations in abrasive waterjet cutting parameters of Lanthanum phosphate/Yttria composite by response surface methodology," *Measurement*, vol. 131, pp. 309–318, 2019.

[24] C. Kalangi, V. Bolleddu, and H. L. Allasi, "Tribological characteristics of carbon nanotubes-reinforced plasma-sprayed Al2O3-TiO2 ceramic coatings," *Advances in Materials Science and Engineering*, vol. 2021, Article ID 8094640, 12 pages, 2021.

[25] A. Borrell, L. Navarro, C. F. Gutiérrez-González, C. Alcázar, M. D. Salvador, and R. Moreno, "Microstructure and mechanical properties of 4YTZP-SiC composites obtained through colloidal processing and Spark Plasma Sintering," *Boletin de la Sociedad Espanola de Ceramica y Vidrio*, vol. 60, no. 3, pp. 175–182, 2021.

[26] A. K. Sharma, R. Bhandari, and C. Pinca-Bretotean, "Impact of silicon carbide reinforcement on characteristics of aluminium metal matrix composite Journal of Physics: Conference," *Series*, vol. 1781, no. 1, Article ID 012031, 2021, February.

[27] M. S. Surya, G. Prasanthi, and S. K. Gugulothu, "Investigation of mechanical and wear behaviour of Al7075/SiC composites using response surface methodology," *Silicon*, vol. 13, no. 7, pp. 2369–2379, 2021.